Infrastructure for the Quantum Internet

Seth Lloyd,[*] Jeffrey H. Shapiro,[†]
and Franco N. C. Wong
Massachusetts Institute of Technology
Research Laboratory of Electronics
77 Massachusetts Avenue
Cambridge, MA 02139

{slloyd@, jhs@, franco@ncw2}.mit.edu

Prem Kumar, Selim M. Shahriar,
and Horace P. Yuen
Northwestern University
Department of Electrical and
Computer Engineering
Center for Photonic Communication
and Computing
2145 North Sheridan Road
Evanston, IL 60208

{kumarp, shahriar, yuen}
@ece.northwestern.edu

ABSTRACT

A team of researchers from the Massachusetts Institute of Technology (MIT) and Northwestern University (NU) is developing a system for long-distance, high-fidelity qubit teleportation. Such a system will be required if future quantum computers are to be linked together into a quantum Internet. This paper presents recent progress that the MIT/NU team has made, beginning with a review of the teleportation architecture and its loss-limited performance analysis.

Categories and Subject Descriptors

B.4.3 [**Input/Output and Data Communications**]: Interconnection (Subsystems); C.2.1 [**Computer Communication Networks**]: Network Architecture and Design; C.2.5 [**Computer Communication Networks**]: Local and Wide-Area Networks

Keywords

Quantum communication, teleportation, qubits, entanglement, quantum memory

1. INTRODUCTION

The physical world is, at bottom, quantum mechanical. Although not directly visible in ordinary life at the human size scale, quantum mechanics has already had a huge effect on our technological society. The quantum states of semiconductor band structure have—with lots of work to develop understanding and the technology—given us integrated circuits and semiconductor lasers. These in turn have fueled

---

[*]Also Department of Mechanical Engineering.

[†]Also Department of Electrical Engineering and Computer Science

the computation and communication revolution that have created the Information Age we live in today. But another revolution may be in the offing, one that could bring us into the Quantum Information Age.

The digital abstraction, on which modern computation and communication rests, admits to only two possible states: a classical on-off system must be in either state 0 or state 1, representing a single bit of information. Quantum mechanics is quite different. A two-level quantum system—the reader unfamiliar with basic quantum mechanics should consult the Appendix for a quick review of all that is needed to understand this paper—can be characterized by two orthogonal basis states (vectors in a Hilbert space) $|0\rangle$ and $|1\rangle$. The system itself, however, may be in an arbitrary superposition of these two states, $\alpha|0\rangle + \beta|1\rangle$, where α and β are complex numbers that satisfy the normalization condition $|\alpha|^2 + |\beta|^2 = 1$. Such arbitrary superpositions represent a single quantum bit of information, i.e., a qubit.

At the micro scale, qubit superposition is innocuous. For example, suppose that the quantum system in question is the polarization of a single photon. Then $|0\rangle$ and $|1\rangle$ might be horizontal and vertical polarization states, respectively. Their equal superpositions, $(|0\rangle \pm |1\rangle)/\sqrt{2}$, then represent $\pm 45°$ linear-polarization states. At the macro scale, on the other hand, things are not so palatable. Take the Schödinger's cat paradox, in which $|0\rangle$ is a live cat and $|1\rangle$ is a dead cat. What possible reality can we ascribe to $(|0\rangle \pm |1\rangle)/\sqrt{2}$, viz., to equal superpositions of life and death?

As if the quantum weirdness of one qubit were not enough, more strange behavior emerges when we move on to two (or more) qubits. The classical behavior of two correlated but random bits is easy to understand, and can be translated into a corresponding qubit situation. But two qubits may be *entangled*, a thoroughly non-classical behavior in which they exist in a superposition of two distinct two-qubit states. Entanglement leads to non-local correlations—spooky action at a distance seemingly in violation of causality—that led Einstein, Podolsky, and Rosen to suggest quantum mechanics might not be complete [1]. Yet, in every experiment in which

superposition and entanglement have been put to the test, quantum mechanics always proves out, which brings us, at last, to quantum computation and quantum communication.

Superposition and entanglement lead to algorithms—for quantum computation—whose performance outstrips the best that can be possibly done with a classical computational algorithm. This advantageous behavior derives from quantum parallelism, whereby superposition allows many computation paths to be explored simultaneously. For example, Grover's algorithm [2], for querying an unsorted database of size N on a quantum computer, affords a $\sqrt{N}$ speedup when compared to its best classical computation competitor. Even more impressive is Shor's factoring algorithm [3], which provides an exponential speedup in comparison with the best known classical approach to factoring. Moreover, just as the Internet opened the door to a vast array of networked applications of classical computing, so too might a network of quantum computers lead to a host of new quantum applications, see e.g., the recent suggestion [4] that the Public Goods Game has a quantum network solution which does not require a trusted third party.

Building a large-scale quantum computer is, at present, an extraordinary and as yet unmet challenge. However, even were many such computers available, linking them together as a quantum network cannot be done with standard fiber-optic Internet infrastructure. The problem is the inscrutable, fragile nature of the qubit. An unknown qubit $\alpha|0\rangle + \beta|1\rangle$ cannot be measured perfectly, i.e., there is no measurement that can divine α and β for an arbitrary qubit. An unknown qubit cannot be cloned [5], i.e., we cannot make multiple copies of an arbitrary $\alpha|0\rangle + \beta|1\rangle$ from a single exemplar. Qubits are also physically fragile, i.e., the state of a two-level quantum system is degraded by interaction with its surrounding environment, such as when our qubit-carrying photon is absorbed or scattered. Collectively, these difficulties place a seemingly impossible hurdle in the path of quantum computer networks. Sharing a quantum algorithm across a network requires that qubits associated with intermediate calculations be shared across that network. This is so because measuring these intermediate-stage qubits will destroy the superpositions and entanglement that give quantum algorithms their speedups. Furthermore, fragility precludes reliable direct long-distance transmission of intermediate-stage qubits. Nevertheless, there is a way out of this bind. If the remote quantum computers can entangle a pair of qubits—one at each site—then with local operations and *classical* communication they can transfer an arbitrary qubit from one to the other by some more quantum weirdness: qubit teleportation [6].

In qubit teleportation the sender (call her Alice) makes a special joint measurement on the qubit to be teleported, $\alpha|0\rangle + \beta|1\rangle$, together with her qubit from the entangled pair she has shared with the receiver (call him Bob). Alice's measurement yields two bits of classical information, namely a message that is equally likely to be any element of $\{00, 01, 10, 11\}$, but no information that she can employ to deduce $\alpha|0\rangle + \beta|1\rangle$. Indeed, after the measurement, the two qubits in Alice's possession will be in a state that is totally independent of the values of α and β. But, entanglement is a very special property. The classical information obtained by Alice from her joint measurement is *exactly* what is needed by Bob to transform his qubit from the original entangled pair into the state $\alpha|0\rangle + \beta|1\rangle$. Amazingly, the four transformations that Bob must employ—depending on which classical message $\{00, 01, 10, 11\}$ he receives from Alice—are completely independent of α and β. Thus, Bob too has no information about the qubit that has been teleported.

In summary, qubit teleportation does not constitute a perfect measurement of an unknown qubit, as neither Alice nor Bob have learned anything about the unknown qubit. Nor does teleportation violate the no-cloning theorem, because Bob cannot create his replica until after Alice's measurement has destroyed the original. Moreover, qubit fragility can be tolerated, because environmental effects only limit the speed with which Alice and Bob can build up a reservoir of entangled qubits for use in teleportation, and precious intermediate-stage computation qubits $\alpha|0\rangle + \beta|1\rangle$ are only manipulated within the confines of the quantum communication element inside Alice's quantum computer. Finally, qubit teleportation does not contradict causality, because classical, light-speed limited, communication from Alice to Bob is intrinsic to the protocol.

In what follows we will describe the approach to long-distance qubit teleportation being pursued by a team of researchers from the Massachusetts Institute of Technology (MIT) and Northwestern University (NU), and review the recent progress that this team has made. Successful completion of this program would provide the basic infrastructure on which a Quantum Internet might be built.

2. TELEPORTATION ARCHITECTURE

As a prelude to our discussion of the MIT/NU architecture, let us quantify the Bennett *et al.* protocol for qubit teleportation [6], whose qualitative structure was spelled out in the Introduction. In advance of undertaking the teleportation operation, Alice and Bob arrange to share a singlet state of two qubits,

$$|\psi^-\rangle_{AB} = (|01\rangle_{AB} - |10\rangle_{AB})/\sqrt{2}, \tag{1}$$

where

$$|01\rangle_{AB} \equiv |0\rangle_A \otimes |1\rangle_B, \tag{2}$$

etc. (We shall see, below, how this sharing can be accomplished with an entangled photon source and trapped-atom quantum memories.) Charlie then supplies Alice with an unknown qubit

$$|\Psi\rangle_C \equiv \alpha|0\rangle_C + \beta|1\rangle_C, \tag{3}$$

asking her to teleport that state to Bob. Alice proceeds as follows. First, she measures the Bell-state observable,

$$\mathcal{B} \equiv \sum_{n=0}^{4} n|B_n\rangle_{AC\,AC}\langle B_n|, \tag{4}$$

on the tensor-product Hilbert space $\mathcal{H}_A \otimes \mathcal{H}_C$, where

$$|B_0\rangle_{AC} \equiv \frac{|10\rangle_{AC} - |01\rangle_{AC}}{\sqrt{2}}, \quad |B_1\rangle_{AC} \equiv \frac{|10\rangle_{AC} + |01\rangle_{AC}}{\sqrt{2}},$$

$$|B_2\rangle_{AC} \equiv \frac{|11\rangle_{AC} - |00\rangle_{AC}}{\sqrt{2}}, \quad |B_3\rangle_{AC} \equiv \frac{|11\rangle_{AC} + |00\rangle_{AC}}{\sqrt{2}}, \tag{5}$$

are the Bell states. Next, she sends Bob the result of her measurement—one of the integers $\{0, 1, 2, 3\}$—as two bits of classical information. This message contains all the information that Bob needs to complete the teleportation process. To see that this is true, we use a little algebra to show that the Alice, Bob, Charlie state prior to Alice's Bell-observable measurement is

$$
\begin{aligned}
|\psi\rangle_{ABC} &= |\psi^-\rangle_{AB} \otimes |\Psi\rangle_C \\
&= \frac{\alpha|0\rangle_B + \beta|1\rangle_B}{2} \otimes |B_0\rangle_{AC} \\
&\quad - \frac{\alpha|0\rangle_B - \beta|1\rangle_B}{2} \otimes |B_1\rangle_{AC} \\
&\quad - \frac{\alpha|1\rangle_B + \beta|0\rangle_B}{2} \otimes |B_2\rangle_{AC} \\
&\quad + \frac{\alpha|1\rangle_B - \beta|0\rangle_B}{2} \otimes |B_3\rangle_{AC}. \quad (6)
\end{aligned}
$$

So, if Alice's Bell-observable outcome is 0, then Bob's state is

$$
|\Psi\rangle_B = \alpha|0\rangle_B + \beta|1\rangle_B, \quad (7)
$$

and nothing needs to be done to complete the teleportation. If her Bell-observable outcome is 1, then Bob completes the teleportation process with a phase-flip operation, i.e., changing the sign of the $|1\rangle_B$ component of his qubit relative to its $|0\rangle_B$ component. If Alice's outcome is 2, then Bob must perform the bit-flip operation, swapping the $|0\rangle_B$ and $|1\rangle_B$ components of his qubit. Finally, if Alice's outcome is 3, Bob must use both the phase-flip and bit-flip operations. Bob need not know anything about α and β to complete the teleportation operation once he is in receipt of Alice's message. Likewise, the Alice-Charlie state *after* she makes the Bell-observable measurement is one of the $\{|B_n\rangle\}$, all of which possibilities have pre-measurement probabilities of $1/4$, so that Alice gleans no information about α and β from her observation.

2.1 Architectural Elements

An initial demonstration of the Bennett *et al.* qubit teleportation protocol was reported by Bouwmeester *et al.* [7],[8], but this work was a table-top experiment in which only one of the Bell states was measured. As a result, only when photodetection clicks heralded the occurrence of that Bell state—a probability $1/4$ event—could the teleportation be completed. Furthermore, this experiment did not include any quantum memory element, so that the teleported state could not be saved for later use. Indeed its presence was demonstrated by an appropriate, but annihilative, measurement procedure.

The Quantum Internet must connect distant quantum computers via teleportation with complete Bell-observable measurements, so as not to sacrifice precious intermediate-stage qubits. Also, it needs quantum memory, for storing a reservoir of entangled qubits and to serve as input and output registers for the teleportation itself. The MIT/NU architecture addresses all of these requirements. Nonlinear optics are used to produce a stream of polarization-entangled photon pairs, i.e., signal and idler photon states of the singlet form

$$
|\psi^-\rangle_{SI} \equiv (|HV\rangle_{SI} - |VH\rangle_{SI})/\sqrt{2}. \quad (8)
$$

The signal and idler photons are routed down L-km-long lengths of standard telecommunication optical fiber—the signal photons proceeding down one fiber and the idler photons down the other—to a pair of quantum memories comprised of ^{87}Rb atoms that are trapped inside high-Q optical cavities [9]. One of these memories belongs to Alice and the other to Bob; the Bell-observable measurements are made in Alice's memory, and the teleportation-completing transformations are performed in Bob's memory. Without delving too much into details, see [10]–[13] for more information, the overall operation can be described in terms of architectural elements shown in Figs. 1–3.

Figure 1(a) shows a simplified energy diagram for the atomic levels in ^{87}Rb that are used in storing the signal and idler qubits from $|\psi^-\rangle_{SI}$ in Alice's memory and Bob's memory, respectively. A photon of arbitrary polarization—expressed as a mixture of left-circular and right-circular components (σ_- and σ_+, respectively) can be absorbed by a rubidium atom that is in the ground state A, transferring its coherence—the α and β values that together characterize its polarization state—to the energy-degenerate excited levels B. By coherently pumping the B-to-D transition with an appropriate laser field, this quantum coherence is transferred to long-lived D levels for storage and processing. Whether or not a photon has been captured in this manner can be verified—in a non-destructive manner—by subsequently pumping the A-to-C cycling transition with another laser field. If the atom has been transferred to the D states, then no fluorescence will be seen on this cycling transition. Thus, Alice and Bob run a time-slotted memory loading protocol in which they repeatedly try to absorb photons, starting over at the end of each trial in which one or both of them see cycling transition fluorescence [12]. By employing an appropriate lattice of such trapped atoms, Alice and Bob can sequentially accumulate a reservoir of shared entanglement for teleporting quantum states between their respective quantum computers.

Figure 1(b) sketches the structure of the entangled photon source in the MIT/NU architecture. It consists of two optical parametric amplifiers (OPAs), viz., resonant optical cavities each containing a second-order ($\chi^{(2)}$) nonlinear crystal in which photon pairs are produced whenever a photon from a strong pump laser of frequency ω_P fissions into a signal photon at frequency ω_S and an idler photon at frequency ω_I. Energy conservation, at the photon level, requires that $\omega_S + \omega_I = \omega_P$. Momentum conservation, at the photon level, requires that the wave vectors associated with the pump, signal, and idler obey $\vec{k}_S + \vec{k}_I = \vec{k}_P$. We assume type-II phase matching, in Fig. 1(b), which forces the signal and idler photons to be orthogonally polarized, as indicated by the bullets and arrows. With proper choice of nonlinear material, each OPA can be made to operate at frequency degeneracy, i.e., the center frequencies of the signal and idler will both be $\omega_P/2$. Making $\omega_P/2$ a cavity resonance for both the signal and the idler polarizations then dramatically increases the resulting signal-idler photon flux within the narrow ($\sim$15 MHz) bandwidth of the ^{87}Rb atomic line. Finally, by combining the outputs from two anti-phased, coherently-pumped OPAs on a polarizing beam splitter (PBS), we obtain the stream of polarization-entangled (singlet-state) photon pairs that are needed.

(a)

(b)
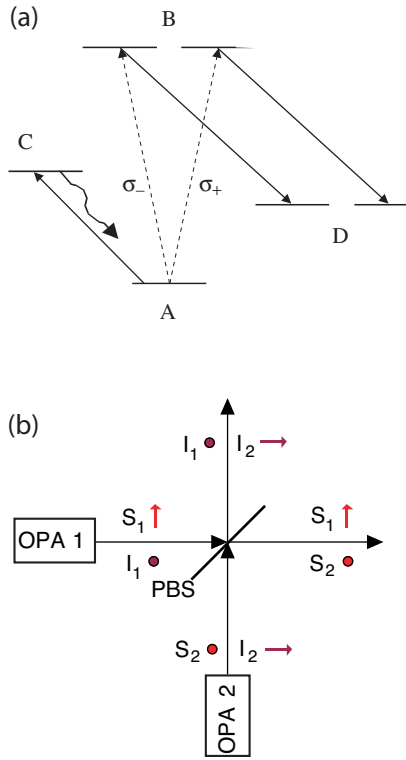
Figure 1: Essential components of the MIT/NU quantum communication architecture: (a) simplified energy-level diagram for the trapped rubidium atom; (b) source of polarization-entangled photon pairs.

The ^{87}Rb-atom quantum memory has its A-to-B absorption line at 795 nm, but low-loss fiber propagation occurs in the 1.5-μm-wavelength window. Furthermore, standard telecommunication fiber does not preserve the polarization state of the light propagating through it. These obstacles to long-distance distribution of polarization-entangled photons to the Rb-atom memories are accounted for, within the MIT/NU architecture, by quantum-state frequency conversion [14] and time-division-multiplexed (TDM) polarization restoration (cf. [15]), as shown in Figs. 2 and 3. In particu-
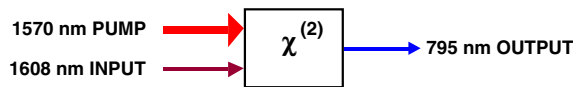
Figure 2: Schematic diagram of quantum-state frequency conversion.

lar, by applying a strong pump beam at 1570 nm to another second-order nonlinear crystal—chosen to satisfy the appropriate phase-matching condition—we can convert a qubit photon received at 1608 nm (in the low-loss fiber transmission window) to a qubit photon at the 795 nm wavelength of the ^{87}Rb quantum memory. For polarization restoration we postpone the PBS combining, shown in Fig. 1(b), until after fiber propagation. This is accomplished by transmitting

time slices from the signal beams from our two OPAs down one fiber in the same linear polarization but in nonoverlapping time slots, accompanied by a strong out-of-band laser pulse. By tracking and restoring the linear polarization of the strong pulse, we can restore the linear polarization of the signal-beam time slices at the far end of the fiber. After this linear-polarization restoration, we then reassemble a time-epoch of the full vector signal beam by delaying the first time slot and combining it on a polarizing beam splitter with the second time slot after the latter has had its linear polarization rotated by 90°. A similar procedure is performed to reassemble idler time-slices after they have propagated down the other fiber.
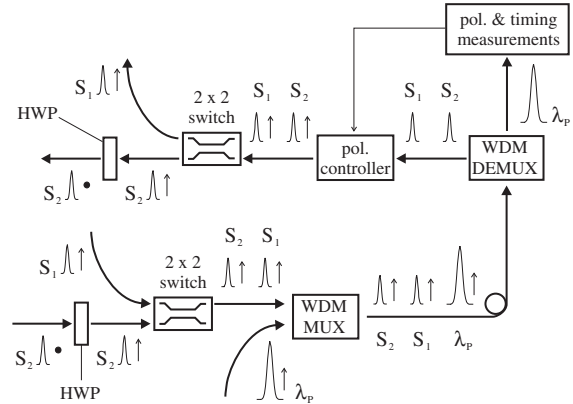

Figure 3: Schematic diagram of time-division-multiplexed polarization restoration for the signal beam. HWP = half-wave plate, WDM MUX = wavelength division multiplexer, WDM DEMUX = wavelength division demultiplexer.

Once Alice and Bob have entangled the atoms within their respective memories by absorbing an entangled pair of photons, the rest of the qubit teleportation protocol is accomplished as follows. Charlie's qubit message is stored in another ^{87}Rb atom, which is trapped in the same optical cavity as Alice's memory atom. By a coherence transfer procedure [16], Charlie inserts his qubit into Alice's memory atom in a manner that permits the Bell-observable measurement to be accomplished by determining in which of four possible states—not shown in Fig. 1(a)—that memory atom now resides. Alice sends the result of her Bell-observable measurement to Bob, who completes the teleportation process by standard atomic level manipulations that realize the phase-flip and bit-flip qubit operations. For details, see [11].

2.2 Basic Performance Analysis

Two key figures of merit can be used to characterize the performance of the MIT/NU qubit teleportation architecture: throughput and fidelity. The former is the number of singlet-states per second that can be accumulated by sequential operation of the quantum-memory loading protocol applied to a lattice of trapped atoms. The latter is the accuracy with which an unknown qubit is replicated by the teleportation process. Figure 4 comprises a throughput/fidelity assessment under rather idealized conditions [12], in which the polarization restoration, Alice's Bell-observable measurement,

and Bob's phase-flip and bit-flip operations are flawless. Included in the calculations underlying Fig. 4 is the propagation loss in the fibers, as well as fixed losses associated with incomplete quantum-state frequency conversion, etc., in each source-to-memory path and the fact that OPA sources can produce multiple photon pairs within a given trial of the memory loading protocol. Fidelity is severely degraded when Alice's memory and Bob's memory absorb photons from different—hence not entangled—photon pairs. The probability of such multiple-pair events is reduced by reducing the pumping level on the OPAs, but this comes at the cost of reducing the throughput, as the rate of single-pair events is also decreased. Figures 4(a) and (b) plot the
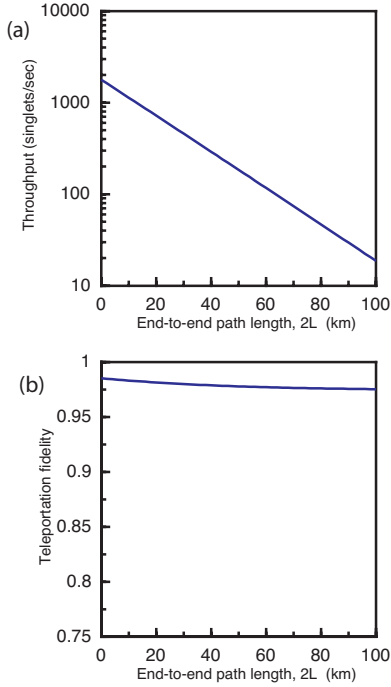
Figure 4: Throughput (singlets/sec) (a) and teleportation fidelity (b) versus end-to-end path length for the MIT/NU architecture. Assumptions and parameter values for these plots are given in the text.

throughput and fidelity, respectively, versus end-to-end path length $2L$. These curves assume that: the loading protocol is run at 500 kHz; the OPAs are pumped at 1% of oscillation threshold; the OPA cavity linewidth is twice the memory cavity linewidth; the fiber loss is 0.2 dB/km; and there is 5 dB of fixed loss in each source-to-memory path. We see that in this ideal, loss-limited performance regime the MIT/NU architecture can sustain throughputs in excess of 100 pairs/sec out to 50 km end-to-end path lengths with teleportation fidelities above 97%.

2.3 Sensitivity Analysis

Although the idealized throughput/fidelity behavior of the MIT/NU architecture is quite promising, it is important to assess how sensitive this performance is to imperfections in the system. Toward that end, we have developed error models [13] that account for a variety of possible degradation mechanisms. Some of the results that we have obtained

from these models are shown in Figs. 5 and 6. In particular, Fig. 5 shows that modest errors in polarization restoration do not appreciably degrade the throughput or the fidelity of the MIT/NU architecture. Here $\cos(\theta_S)$ and $\cos(\theta_I)$ are transmission factors projecting the imperfectly polarization restored signal and idler photons onto the reference polarization in Fig. 3. Interestingly, polarization-restoration errors have virtually no effect on fidelity, although they must be kept well below 1 rad to minimize throughput loss.

Figure 6(a) addresses the impact of improperly phased pump beams—$\Delta\psi = 0$ is the desired anti-phased situation that produces singlet states—in the dual-OPA source shown in Fig. 1(b). At $\Delta\psi = \pi$ the pumps are in phase, thus producing a stream of triplet states,

$$|\psi^+\rangle_{SI} \equiv (|HV\rangle_{SI} + |VH\rangle_{SI})/\sqrt{2}, \qquad (9)$$

from the dual-OPA. Alice and Bob, however, are performing teleportation under the assumption that they are sharing a singlet state; the phase flip that changes the singlet $|\psi^-\rangle_{SI}$ into $|\psi^+\rangle_{SI}$ is therefore not accounted for and the result is a disastrous loss of fidelity. However, keeping the pump-phase error well below 1 rad—something that is easily accomplished experimentally—will ensure that near-peak fidelity is maintained. Figure 6(b) shows the fidelity loss that arises from there being Gaussian-distributed pump gain fluctuations in the dual-OPA source. These fluctuations are taken to have variance σ_G^2 about a mean gain $G = 0.1$, corresponding to operation at 1% of oscillation threshold. We see that realistic 1% pump-power fluctuations, corresponding to $\sigma_G^2 = 10^{-4}$, lead to minimal performance loss.

3. PROGRESS ON ENTANGLEMENT GENERATION AND TRANSMISSION

3.1 $\chi^{(2)}$ Sources

The dual-OPA entanglement source of Fig. 1(b) can be easily implemented using a single $\chi^{(2)}$ nonlinear optical crystal with bidirectional pumping. The dual-pump single-crystal configuration ensures that the two counter-propagating light beams generated from the two coherently driven OPAs are truly identical, thus allowing the outputs to be combined interferometrically at the polarizing beam splitter in Fig. 1(b). We have recently demonstrated this dual-pump system using a periodically-poled potassium titanyl phosphate (PPKTP) crystal for generating polarization-entangled photons with a flux of over 10 000 detected pairs/s/mW of pump power with a quantum-interference visibility of over 90% [17]. The PPKTP source has signal and idler outputs at ~795 nm for loading local Rb-based quantum memories and a spectral bandwidth of 500 GHz.
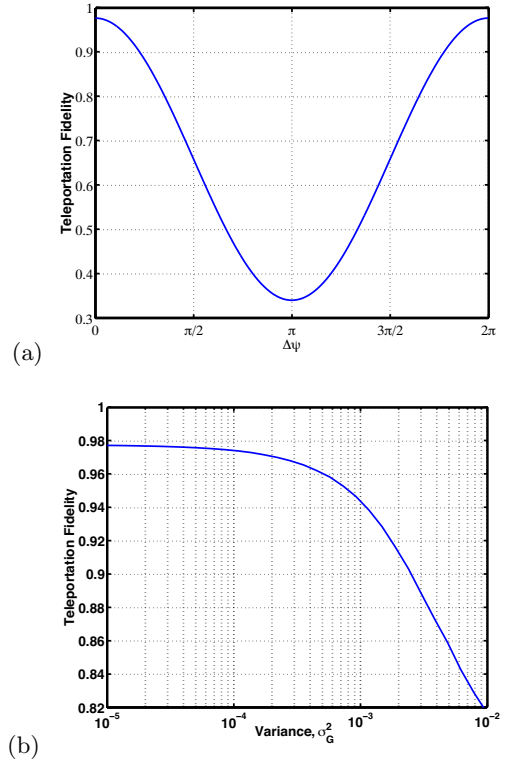
The PPKTP source, however, is not suitable for our long-distance teleportation architecture because fiber-optic transmission at 795 nm would be lossy (more than 5 dB/km compared with 0.2 dB/km at 1550 nm) and the source is too broadband for an atom-based quantum memory whose bandwidth is tens of MHz. To minimize the transmission loss in optical fibers and to increase the spectral brightness of the source, we have developed an even more efficient entanglement source—using a periodically poled lithium niobate (PPLN) crystal—with outputs at 795 nm and 1608 nm [18], shown schematically in Fig. 7. With two vastly different out-

(a)

(b)
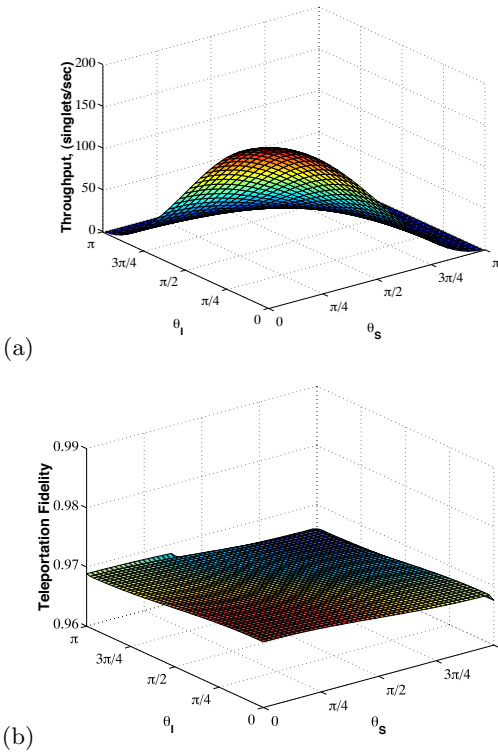
Figure 5: Throughput (singlets/sec) (a) and teleportation fidelity (b) versus polarization-restoration error angles. These plots assume a 50 km end-to-end path length; other assumptions and parameter values for these plots are as given for Fig. 4.


(a)

(b)

Figure 6: Teleportation fidelity versus pump phase error (a) and pump-gain variance (b). These plots assume a 50 km end-to-end path length; other assumptions and parameter values for these plots are as given for Fig. 4.

put wavelengths, the bidirectionally pumped PPLN source is suitable for loading a local quantum memory at 795 nm and a remote quantum memory accessed via fiber-optic transport of the 1608 nm photons and quantum-state frequency conversion. Fiber-optic delivery offers the additional advantage of confining photons to a well-defined spatial mode that can be matched to what is required for the quantum memories.

The output wavelengths of the PPLN entanglement source may be selected, by choice of the crystal's grating period, and tuned, by changing its temperature. With high efficiency (10^7 pairs/s) and wavelength tunability, this source [19] is compatible with quantum memories using different atomic species (each with a different wavelength). The PPLN output state can be set to one of the four Bell states by controlling the relative phase of the various output path lengths, accomplished by translating the position of one of the mirrors in the beam paths. Figure 7(b) shows the maximum and minimum coincidence rates after the light beams pass through polarization analyzers at different mirror sweep positions (as a function of time). It shows that it is possible to work at any desired polarization-entangled output state, such as the singlet state. Single spatial mode fiber delivery of the photons has another intrinsic advantage: the amount of light being collected by the $\sim$10-μm-diameter optical fiber acts as a spectral filter. This occurs because emission angle is correlated with emission frequency

for the PPLN source. We have thus observed a much smaller ($\sim$50 GHz) bandwidth for the fiber-coupled PPLN source at a spectral brightness of 320 pairs/s/GHz/mW of pump. By using a 100-mW pump and a commercially available first-order grating PPLN crystal (instead of the third-order grating in the present setup) the source can be scaled to yield a polarization-entangled pair generation rate of $\sim$16 000/s in a 50 MHz bandwidth. Together with quantum-state frequency conversion, such a source is suitable for loading remote quantum memories.

3.2 $\chi^{(3)}$ **Sources**

Despite the success reported in the previous section, it is still the case that efficient coupling into optical fiber of the entangled photons produced in bulk nonlinear crystals poses a significant challenge [21]. Therefore, a source emitting entangled photons directly in the fiber is desirable, preferably in the low-loss transmission band of standard silica fibers near 1550 nm wavelength. We have recently developed such a source by exploiting the $\chi^{(3)}$ (Kerr) nonlinearity of the fiber itself [22]. When a pump pulse is injected into a fiber at a wavelength close to the zero-dispersion point, inelastic four-photon scattering (FPS) is significantly enhanced. In this process, two pump photons at frequency ω_p scatter through the Kerr nonlinearity of the fiber to create energy-time entangled Stokes (signal) and anti-Stokes (idler) photons at frequencies ω_s and ω_a, respectively, such that $2\omega_p = \omega_s + \omega_a$.
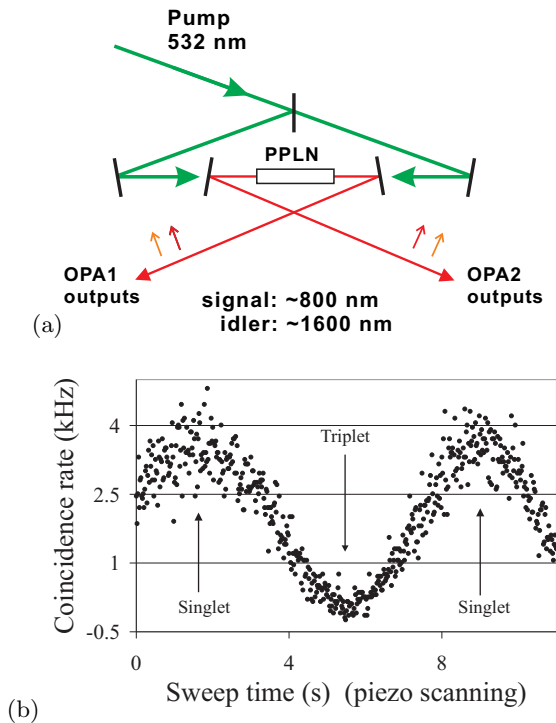
Figure 7: (a): Schematic diagram of dual-pumped nondegenerate PPLN downconverter. Signal and idler from each output beam are combined by polarizing beam splitters after the polarization of one of the two beams undergoes 90° rotation. (b): Coincidence rate versus timed sweep of phase-controlling mirror showing different entanglement states that can be achieved. Polarizers at the detectors were set orthogonal and accidental counts were subtracted.

The isotropic nature of the Kerr nonlinearity in fused-silica-glass fiber makes these correlated, scattered photons predominantly co-polarized with the pump. Thus, by coherent combination of outputs from two orthogonally-polarized parametric processes we have produced polarization entanglement [23]. Indeed, all four Bell states were prepared, and Bell's inequality violations of up to 10 standard deviations of measurement uncertainty were demonstrated [23]. In early experiments with this source, the total number of coincidence counts between the Stokes and anti-Stokes photons exceeded the number of accidental coincidences by only a factor of 2.5 [22]. We have recently shown that spontaneous Raman scattering accompanying FPS causes this problem. By reducing the detuning between the Stokes and pump photons, we have been able to show (see Fig. 8) that the accidental coincidences can reduced to less than 10% of the true coincidences at a production rate of about 0.04 photon-pairs/pulse [24]. Hence, this fiber source should yield a two-photon quantum interference visibility in excess of 85% *without* subtracting the accidental coincidences.

To demonstrate the utility of our fiber-based source of polarization entangled photons [23] for long-distance entanglement distribution, we separated the Stokes and anti-Stokes photons—which are entangled in polarization but have different wavelengths—by use of an optical filter and launched
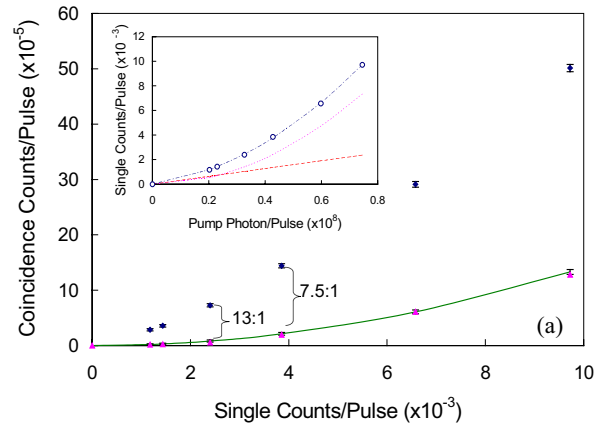
Figure 8: Measured coincidence rate versus number of scattered photons per pump pulse (labelled Single Counts/Pulse) in the anti-Stokes channel for scattered photons co-polarized with the pump. The diamonds represent the total-coincidence counts produced by a single pump pulse and the triangles represent the coincidence counts produced by two adjacent pump pulses. The latter measures the accidental coincidences contributing to the total and is well fitted by the line, which is a plot of the product of the photon counts in the Stokes and anti-Stokes channels produced by the adjacent, i.e., independent, pump pulses. The inset shows the number of scattered photons per pump pulse detected in the anti-Stokes channel as a function of the number of photons in the pump pulse (hollow circles). Taking into account the detection efficiency of 6% in the anti-Stokes channel, at a photon-pair production rate of 0.04 (0.067) per pulse the ratio between the total coincidence rate and the accidental coincidence rate is 13:1 (7.5:1). See [24] for further details.

them into separate 25-km-long spools of commercially available single-mode fibers (Corning SMF-28 and Corning LEAF), as shown schematically in Fig. 9(a). The propagation loss through each spool of fiber was measured to be approximately 0.2 dB/km. Fiber polarization controllers were spliced into the photon propagation path at the end of each spool and test pulses of known polarization states were used to align the polarization axes (horizontal and vertical) at the input and output ends of the two fibers. A polarizer was used at the output end of each fiber to project the polarization state of the emerging photon to 45° relative to the vertical.

After 25 km of propagation in separate spools of fiber, the emerging Stokes and anti-Stokes photons were detected in coincidence to measure quantum interference as a function of the relative phase ϕ_p between the two pump pulses that created the polarization entanglement. (Appropriate delays in the photon-counting electronics were introduced to account for the propagation in the two fibers.) The results are shown in Fig. 9(b): no interference is observed in the single counts, whereas high-visibility (86%) interference is observed in the coincidence counts. These results clearly show that high-fidelity polarization entanglement can sur-
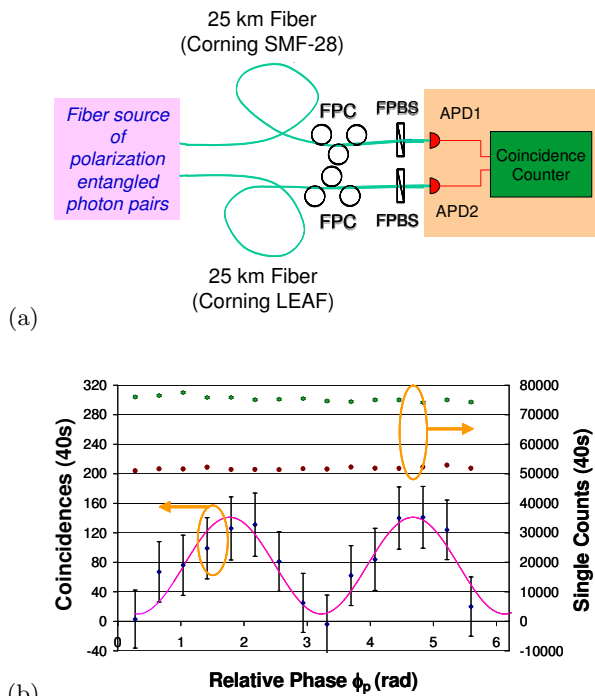
(a)

(b)

Figure 9: (a): Schematic of the experimental setup to demonstrate long-distance entanglement distribution. FPC, fiber polarization controller; FPBS, fiber-pigtailed polarization beam splitter; APD, avalanche-photodiode based photon-counting detector. (b): Single counts (right ordinate) and coincidence counts (left ordinate) registered by the detectors of Stokes and anti-Stokes photons versus the relative phase between the source's two pump pulses. The contribution of accidental coincidences has been subtracted.

vive 50 km end-to-end fiber propagation [25].

4. QUANTUM-STATE FREQUENCY CONVERSION

The MIT-NU architecture requires that fiber-delivered photons at 1.55–1.6 μm wavelength be upconverted to the 795 nm wavelength of the Rb-atom memory with high efficiency and in a manner that preserves their polarization state. Figure 3 shows a time-division-multiplexed scheme for transmitting an arbitrary polarization state down an optical fiber with high fidelity. Even though the scheme has yet to be demonstrated for a single-photon input, the required components and technologies, such as fast switches and wavelength division multiplexing and demultiplexing, are readily available in the telecommunication industry. If the frequency translation step is performed just before the outputs are reassembled, the polarizations of the two components (S_1 and S_2 in Fig. 3) are known and the same, and hence only a single stage of frequency upconversion is needed.

We have recently demonstrated 90%-efficient single-photon upconversion from 1.55 μm to 631 nm by sum-frequency mixing [20]; Fig. 10(a) shows the basic scheme. A strong pump laser at 1064 nm is resonated in a ring cavity to sustain a

high circulating pump power within the cavity, reaching a maximum of 22 W. The intracavity pump mixes with an input photon at 1.55 μm in a PPLN crystal to generate a photon at 631 nm. Our 90% efficiency is limited by inadequate pump power ($\sim$35 W is required for complete upconversion), but the results clearly demonstrate the viability of our upconversion scheme. Figure 10(b) plots the upconversion efficiency versus circulating pump power. We have observed a significant amount of background photocounts, due to pump-induced fluorescence which is upconverted into the same spectral and spatial mode as the signal photons. While these background counts do not significantly affect the teleportation architecture, they can be eliminated by using a longer-wavelength pump laser.
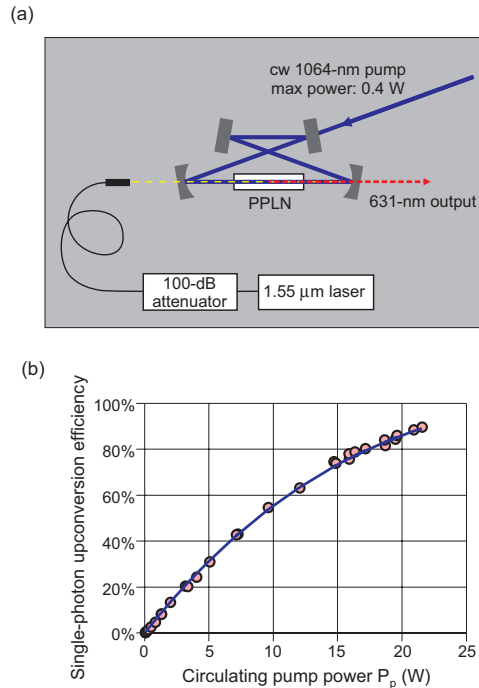
(a)

(b)

Figure 10: Frequency upconversion: (a) schematic of sum-frequency mixing upconversion with a ring cavity configuration for the continuous-wave (cw) pump; (b) single-photon upconversion efficiency.

5. TRAPPED ATOM QUANTUM MEMORY

An essential ingredient for the MIT/NU architecture is a quantum memory unit (QMU) embodied by a single ^{87}Rb atom trapped inside a high-finesse optical cavity: it entails a strong coupling between a single atom and a single photon with a very small mode volume. Figure 11(a) illustrates the basic concept behind our single-atom QMU. The atom is to be caught in a three-dimensional dipole force trap, conventionally known as a FORT (far off-resonance trap). Upon capture in this trap, the atom is to be further cooled down to the ground state of its center-of-mass motion. The cavity is formed by a pair of curved mirrors, each with a reflectivity as high as 99.998%, with a separation of less than 100 μm. In Fig. 11(b), we show one of several custom designed optomechanical devices we have developed in order to realize this geometry. The piezo-electric elements are needed to lock the

(a)

(b)
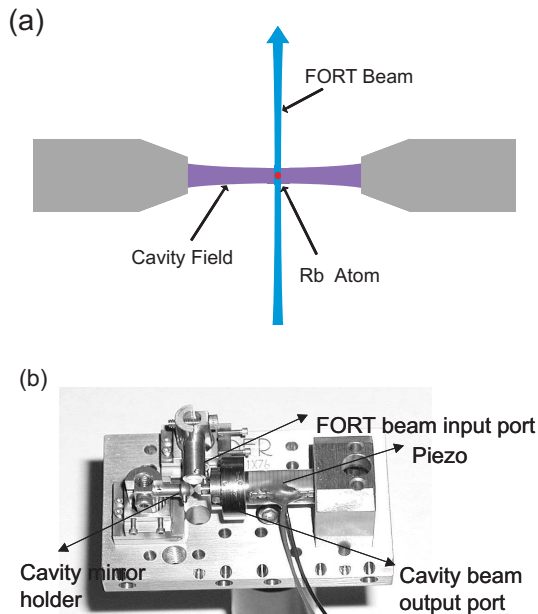
Figure 11: (a) Schematic of the trapped-atom QMU; (b) integrated cavity-FORT for realizing the QMU.

cavity to the optical transition of interest. The whole system has to be operated under an ultra-high vacuum, in order to ensure that the atom does not collide with residual gas and get ejected from the trap.

To isolate and cool a single atom to the point that it can be trapped in the FORT requires several steps. First, solid rubidium is heated to produce an atomic vapor and then passed through a pair of nozzles to produce an atomic beam. The atoms in this beam are slowed to a few m/s using resonant radiation pressure from a diode laser, and then cooled and trapped in a magneto-optic trap (MOT). Because the MOT cannot be co-located with the cavity-FORT unit, we transfer the atoms from one to the other using the following launch-and-catch approach. We apply a pulse of radiation pressure to create an atomic fountain that is arranged to make the atoms come to rest at the center of the cavity-FORT unit, at which point the FORT is enabled. A collisional blockade, or its equivalent, is then used to ensure that the FORT contains only one atom. Finally, a Raman cooling process is used to cool the atom to its motional ground state.

We have built two separate vacuum chambers in order to realize the two QMU's needed for demonstrating the qubit teleportation process. In each chamber, the atoms are cooled and trapped in a MOT in an identical fashion after which they undergo launch-and-catch into the cavity-FORT units. The distance between the MOT and the cavity-FORT is greater in one chamber than it is in the other, so we have added a quadrupolar magnetic-wire guide to the longer-distance QMU to ensure a significant atomic flux into its cavity. Figure 12 shows a typical launch-and-catch process. Figure 12(a) shows a cloud of atoms after they were launched into a FORT. Figure 12(b) shows the line density
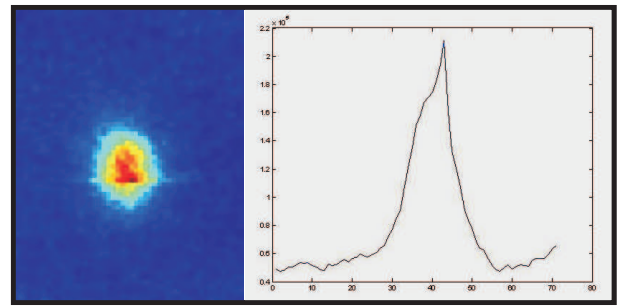
Figure 12: Launch-and-catch process using a FORT beam: (a) launched atomic cloud after the FORT is turned on; (b) atomic density integrated horizontally.
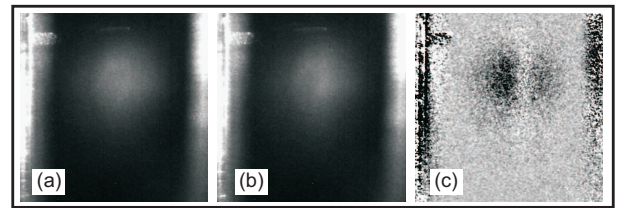
Figure 13: Preliminary performance of the quadrupolar wire guide: (a) atomic cloud without guide; (b) atomic cloud with guide; (c) difference between the clouds in (a) and (b).

of atoms integrated horizontally, with the spike occurring at the FORT location. As time progresses, most of the atoms fall, except for the ones caught in the FORT. Figure 13 shows the preliminary performance of our quadrupolar wire guide. Figure 13(a) shows the atom cloud after launch, looking from the side, without the guide turned on. Figure 13(b) shows the same cloud with the guide turned on. Figure 13(c) is the difference between these two cases, showing a compression of the atomic density towards the center. The guiding shown here is not very pronounced, because the guiding wires were far apart at the measurement location. We are currently reconfiguring our imaging system to see the atoms at a location where the wires are closer together. The next step is to install the cavity-FORT integrated structure inside the vacuum chamber. Once this is achieved, we still face the challenge of ensuring that only a single atom is trapped in each FORT, and that it can be cooled to the motional ground state.

6. CONCLUSION

We have reported a complete architecture—and progress towards its instantiation—for long-distance, high-fidelity qubit teleportation that, if successfully realized, could provide the quantum communication infrastructure needed for a Quantum Internet.

ACKNOWLEDGMENT

APPENDIX

Here we shall present a bare bones introduction to the quantum mechanics needed to understand qubit teleportation. Because the MIT/NU architecture relies on entangled photons, we also include a similarly minimal treatment for the quantum behavior of a single-mode electromagnetic field. For readers desiring a more complete introduction to the quantum mechanics of qubits, the text by Nielsen and Chuang is recommended [26]; readers seeking more information about quantized electromagnetic fields may consult the text by Louisell [27].

Quantum States and Quantum Measurements

A quantum mechanical system is a physical system governed by the laws of quantum mechanics. Its state is the sum total of all the information that can be known about that system. In Dirac notation, the state of a quantum system is represented by a ket vector $|\psi\rangle$ in the Hilbert space $\mathcal{H}$ of possible states for that system. For calculations we need the bra (adjoint) vector, $\langle\psi|$ associated with the state, so that we can evaluate the inner (dot) product between two states $|\psi\rangle$ and $|\psi'\rangle$ as the "bra-ket" $\langle\psi|\psi'\rangle$. In particular, finite-energy states all have unit length, viz., $\langle\psi|\psi\rangle = 1$.

It is convenient to regard $|\psi\rangle$ as a column vector and $\langle\psi'|$ as a row vector, in terms of some orthonormal basis for $\mathcal{H}$. For a single qubit this is especially simple, as the underlying Hilbert space is two dimensional. Consider the single photon discussed in the Introduction. An orthonormal basis for its Hilbert space of polarization states is provided by the horizontal and vertical polarization states, which here will be denoted $|H\rangle$ and $|V\rangle$, viz., these states satisfy

$$\langle H|H\rangle = \langle V|V\rangle = 1 \quad \text{and} \quad \langle H|V\rangle = \langle V|H\rangle = 0, \quad (10)$$

and all states in $\mathcal{H}$ can be expressed as superpositions—with, in general, complex-number coefficients—of $|H\rangle$ and $|V\rangle$. Thus by regarding arbitrary polarization-state kets $|\psi\rangle$ and $|\psi'\rangle$ as column vectors,

$$|\psi\rangle \leftrightarrow \begin{bmatrix} \alpha \\ \beta \end{bmatrix} \quad \text{and} \quad |\psi'\rangle \leftrightarrow \begin{bmatrix} \alpha' \\ \beta' \end{bmatrix}, \quad (11)$$

and their associated polarization-state bras $\langle\psi|$ and $\langle\psi'|$ as row vectors,

$$\langle\psi| \leftrightarrow \begin{bmatrix} \alpha^* & \beta^* \end{bmatrix} \quad \text{and} \quad \langle\psi'| \leftrightarrow \begin{bmatrix} \alpha'^* & \beta'^* \end{bmatrix}, \quad (12)$$

where * denotes complex conjugation, standard linear algebra yields

$$\langle\psi|\psi'\rangle = \begin{bmatrix} \alpha^* & \beta^* \end{bmatrix} \begin{bmatrix} \alpha' \\ \beta' \end{bmatrix} = \alpha^*\alpha' + \beta^*\beta' \quad (13)$$

for their inner product, whence $|\alpha|^2 + |\beta|^2 = 1$ for a finite-energy state $|\psi\rangle$. For more complicated situations—like the single-mode electromagnetic field discussed below—an infinite-dimensional Hilbert space may be involved.

A little more linear algebra crops up in the specification of quantum measurements. Here we shall limit our remarks to the case of observables [27]—as opposed to the more general case of probability operator-valued measures [26]—because they suffice for the Bell-state measurements needed in qubit teleportation. Observables are physically measurable properties of a quantum system. They are represented by Hermitian operators on the Hilbert space of states, hence they have real-valued eigenvalues and orthonormal eigenkets, with the latter constituting a basis for $\mathcal{H}$. If we measure an observable $\mathcal{O}$—with eigenvalues $\{o_n\}$ and orthonormal eigenkets $\{|o_n\rangle\}$—the outcome will be one of the eigenvalues and, assuming that the eigenvalues are distinct (which is the only case we will require), the probability of getting the outcome o_n, given that the quantum system was in state $|\psi\rangle$ immediately before the measurement, is $\Pr(o_n \mid |\psi\rangle) = |\langle o_n|\psi\rangle|^2$. Note that the absolute phase of a state vector is irrelevant, $|\psi\rangle$ and $e^{i\theta}|\psi\rangle$ have the same measurement statistics. More importantly, for non-annihilative measurements, the state of the system immediately after o_n is obtained from measuring $\mathcal{O}$ will be the associated eigenket $|o_n\rangle$.

A simple example of an observable measurement is the following. A single photon in an arbitrary polarization state is applied at the input to a polarizing beam splitter (PBS), whose horizontally and vertically polarized outputs are detected by ideal photon counters. The difference between the horizontal and vertical counts is the observable

$$\mathcal{O} \equiv |H\rangle\langle H| - |V\rangle\langle V|, \quad (14)$$

i.e., it has eigenvalues $\{+1, -1\}$ and associated eigenkets $\{|H\rangle, |V\rangle\}$. Note that this measurement is annihilative, i.e., the photon is destroyed in the process of the measurement, so we cannot speak of the photon's state after the $\mathcal{O}$ measurement.

The final concept we require from basic quantum mechanics is the tensor product structure employed to characterize multiple quantum systems. Suppose we have a pair of photons—denoted S and I for signal and idler, a terminology derived from the sources we use in the MIT/NU architecture—whose polarization qubits are to provide the entanglement resource needed for qubit teleportation. Using $\mathcal{H}_S$ and $\mathcal{H}_I$ to denote their respective Hilbert state spaces, we define their joint state space to be the tensor product space $\mathcal{H} \equiv \mathcal{H}_S \otimes \mathcal{H}_I$. An arbitrary state in this tensor-product space is a superposition of tensor products of the basis states from the signal and idler state spaces, namely,

$$\begin{aligned} |\psi\rangle &= \alpha|H\rangle_S \otimes |H\rangle_I + \beta|H\rangle_S \otimes |V\rangle_I \\ &+ \gamma|V\rangle_S \otimes |H\rangle_I + \delta|V\rangle_S \otimes |V\rangle_I \\ &= \alpha|HH\rangle + \beta|HV\rangle + \gamma|VH\rangle + \delta|VV\rangle, \quad (15) \end{aligned}$$

where the second equality provides a convenient shorthand. The state $|\psi\rangle$ is said to be a product state if it factors into the tensor product of a state $|\psi\rangle_S$ on $\mathcal{H}_S$ times a state $|\psi\rangle_I$ on $\mathcal{H}_I$; such will be the case in the preceding equation if and only if

$$\alpha = \alpha_S\alpha_I \quad \beta = \alpha_S\beta_I \quad \gamma = \beta_S\alpha_I \quad \delta = \beta_S\beta_I \quad (16)$$

for some $\{\alpha_S, \beta_S, \alpha_I, \beta_I\}$. The inner product of two product states $|\psi\rangle$ and $|\psi'\rangle$ is given by

$$\langle\psi|\psi'\rangle = (_S\langle\psi|\psi'\rangle_S)(_I\langle\psi|\psi'\rangle_I). \quad (17)$$

If $|\psi\rangle \in \mathcal{H} = \mathcal{H}_S \otimes \mathcal{H}_I$ is *not* a product state, then it is entangled. By linearity, inner products between two entangled states on $\mathcal{H}$ can be built up from (15) using the definition for product states.

Quantization of the Single-Mode Electromagnetic Field

The throughput and fidelity analyses reported in Sec. II depend on a full quantum treatment for the electromagnetic field. Even though we did not include the details of that development, it is still of value to supply some of the foundational concepts here. A propagating electromagnetic wave may be decomposed into a collection of modes, e.g., by selecting particular values for the frequency, direction of propagation, and polarization. Quantization of each mode then leads, in turn, to a quantum description for the full field. Any particular mode has equations of motion that mimic those of the harmonic oscillator. Its state space is spanned by orthonormal eigenkets $\{\,|n\rangle : n = 0, 1, 2, \ldots, \}$ that are known as photon-number states, because $|n\rangle$ is a state containing exactly n photons. An ideal photon-counting measurement made on this single mode field is thus represented by the observable

$$\mathcal{N} = \sum_{n=0}^{\infty} n|n\rangle\langle n|. \tag{18}$$

Standard optical sources do not produce photon-number states. In particular, the single-mode field from a laser can approximate the coherent state,

$$|\alpha\rangle \equiv \sum_{n=0}^{\infty} \frac{\alpha^n}{\sqrt{n!}} e^{-|\alpha|^2/2}|n\rangle; \tag{19}$$

so that a photon-counting measurement on this state then yields the familiar Poisson distribution that classical physics associates with shot noise:

$$\Pr(\,n \mid |\alpha\rangle\,) = \frac{|\alpha|^{2n}}{n!} e^{-|\alpha|^2}, \quad \text{for } n = 0, 1, 2, \ldots \tag{20}$$

Nonlinear optics in second-order ($\chi^{(2)}$) or third-order ($\chi^{(3)}$) media can produce signal and idler modes in the entangled state

$$|\psi\rangle = \sum_{n=0}^{\infty} \sqrt{\frac{\bar{N}^n}{(\bar{N}+1)^{n+1}}}\,|n\rangle_S \otimes |n\rangle_I, \tag{21}$$

where $\bar{N}$ is the average photon number in each mode. When $\bar{N} \ll 1$, this state reduces to the simpler form,

$$|\psi\rangle \approx \sqrt{\frac{1}{\bar{N}+1}}|00\rangle + \sqrt{\frac{\bar{N}}{(\bar{N}+1)^2}}(|01\rangle + |10\rangle). \tag{22}$$

Generalizing this state—to two polarizations modes (H and V) each for the signal and the idler—then provides the entangled-photon pair needed for the MIT/NU architecture, because the trapped-atom quantum memories permit the vacuum state (zero-photon) component $|00\rangle$ to be ignored.

7. REFERENCES

[1] A. Einstein, B. Podolsky, and N. Rosen, "Can quantum-mechanical description of physical reality be considered complete?," Phys. Rev. **47**, 777–780 (1935).

[2] L. Grover, "Quantum mechanics helps in searching for a needle in a haystack," Phys. Rev. Lett. **79**, 325–328 (1997).

[3] P. W. Shor, "Algorithm for quantum computation: discrete logarithms and factoring," in *Proceedings 35th Annual Symposium of Foundations of Computer Science*, IEEE Press, Los Alamitos, CA, 1994.

[4] K.-Y. Chen, T. Hogg, and R. Beausoleil, "A practical quantum mechanism for the public goods game," e-print quant-ph/0301013

[5] W. K. Wootters and W. H. Zurek, "A single quantum cannot be cloned," Nature **299**, 802–803 (1982).

[6] C. H. Bennett, G. Brassard, C. Crépeau, R. Jozsa, A. Peres, and W. K. Wootters, "Teleporting an unknown quantum state via dual classical and Einstein-Podolsky-Rosen channels," Phys. Rev. Lett. **70**, 1895–1899 (1993).

[7] D. Bouwmeester, J.-W. Pan, K. Mattle, M. Eibl, H. Weinfurter, and A. Zeilinger, "Experimental quantum teleportation," Nature **390**, 575–569 (1997).

[8] D. Bouwmeester, K. Mattle, J.-W. Pan, H. Weinfurter, A. Zeilinger, and M. Zukowski, "Experimental quantum teleportation of arbitrary quantum states," Appl. Phys. B, **67**, 749–752 (1998).

[9] For ease of calculation, without appreciable loss of generality, our architectural analysis relies on a symmetric arrangement, wherein the entanglement source is equidistant from the two trapped-atom memories. In actual implementation the source will be co-located with one of these quantum memories.

[10] J. H. Shapiro and N. C. Wong, "An ultrabright narrowband source of polarization-entangled photon pairs," J. Opt. B: Quantum Semiclass. Opt. **2**, L1–L4 (2000).

[11] S. Lloyd, M. S. Shahriar, J. H. Shapiro, and P. R. Hemmer, "Long-distance, unconditional teleportation of atomic states via complete Bell state measurements," Phys. Rev. Lett. **87**, 167903 (2001).

[12] J. H. Shapiro, "Architectures for long-distance quantum communication," New J. Phys. **4**, 47 (2002).

[13] B. J. Yen and J. H. Shapiro, "Error models for long-distance qubit teleportation," IEEE J. Selected Topics in Quantum Electron. **9**, 1483–1494 (2003).

[14] P. Kumar, "Quantum frequency conversion," Opt. Lett. **15**, 1476–1478 (1990); J. M. Huang and P. Kumar, "Observation of quantum frequency conversion," Phys. Rev. Lett. **68**, 2153–2156 (1992).

[15] K. Bergman, C. R. Doerr, H. A. Haus, and M. Shirasaki, "Sub-shot-noise measurement with fiber-squeezed optical pulses," Opt. Lett. **18**, 643–645 (1993).

[16] T. Pellizzari, S. A. Gardiner, J. I. Cirac, and P. Zoller, "Decoherence, continuous observation, and quantum computing: a cavity-QED model," Phys. Rev. Lett. **75**, 3788–3791 (1995).

[17] M. Fiorentino, G. Messin, C. E. Kuklewicz, F. N. C. Wong, and J. H. Shapiro, "Generation of ultrabright tunable polarization entanglement without spatial, spectral, or temporal constraints," Phys. Rev. A **69**, 041801(R) (2004).

[18] E. J. Mason, M. A. Albota, F. König, and F. N. C. Wong, "A frequency-nondegenerate entanglement source using periodically poled lithium niobate," in J. H. Shapiro and O. Hirota, eds., *Proceedings of the Sixth International Conference on Quantum Communication, Measurement and Computing* (Rinton Press, Princeton 2003), pp. 107–110.

[19] E. J. Mason, M. A. Albota, F. König, and F. N. C. Wong, "Efficient generation of tunable photon pairs at 0.8 and 1.6 μm," Opt. Lett. **27**, 2115 (2002).

[20] M. A. Albota and F. N. C. Wong, "Efficient single-photon counting at 1.55 μm by means of frequency upconversion," Opt. Lett. **29**, 1449 (2004).

[21] F. A. Bovino, P. Varisco, A. M. Colla, G. Castagnoli, G. Di Giuseppe, and A. V. Sergienko, "Effective fiber-coupling of entangled photons for quantum communication," Opt. Commun. **227**, 343–348 (2003).

[22] M. Fiorentino, P. L. Voss, J. E. Sharping, and P. Kumar, "All-fiber photon-pair source for quantum communication," IEEE Photon. Technol. Lett. **27**, 491–493 (2002).

[23] X. Li, P. L. Voss, J. E. Sharping, and P. Kumar, "Optical-fiber source of polarization-entangled photon pairs in the 1550 nm telecom band," submitted to Phys. Rev. Lett., e-print quant-ph/040219.

[24] X. Li, J. Chen, P. L. Voss, J. E. Sharping, and P. Kumar, "All-fiber photon-pair source for quantum communications: Improved generation of correlated photons," Opt. Express **12**, 3737–3744 (2004).

[25] X. Li, P. L. Voss, J. Chen, J. E. Sharping, and P. Kumar, "Storage and long-distance distribution of polarization entanglement generated in the telecom band of standard optical fiber," in preparation for submission to Optics Letters.

[26] M. A. Nielsen and I. L. Chuang, *Quantum Computation and Quantum Information* (Cambridge Univ. Press, Cambridge, 2000).

[27] W. H. Louisell, *Quantum Statistical Properties of Radiation* (Wiley, New York, 1973).